Advances in Science and Technology Research Journal

Advances in Science and Technology Research Journal 2022, 16(4), 318–326
https://doi.org/10.12913/22998624/153444
ISSN 2299-8624, License CC-BY 4.0

Received: 2022.07.20
Accepted: 2022.08.24
Published: 2022.09.05

Thermal Desorption of Argon Implanted into Gallium Arsenide

Marcin Turek[1], Andrzej Droździel[1], Krzysztof Pyszniak[1*], Paweł Węgierek[2]

[1] Institute of Physics, Maria Curie Sklodowska University in Lublin, Pl. M. Curie-Sklodowskiej 1, 20-031 Lublin, Poland

[2] Faculty of Electrical Engineering and Computer Science, Lublin University of Technology, Nadbystrzycka 38A, 20-618 Lublin, Poland

* Corresponding author's e-mail: kpysz1@o2.pl

ABSTRACT

Thermal desorption of Argon (Ar) implanted with energies 150 keV and 100 keV with fluence 1×10^{16} cm^{-2} into gallium arsenide is considered. A sudden release of Ar is observed in temperature range 1100–1180 K as a single narrow peak in TDS (Thermal Desorption Spectroscopy) spectra. This is accompanied by a strong background signal from atmospheric Ar trapped in various parts of the spectrometer. Desorption peak shift analysis allows estimation of desorption activation energy values – these are 3.6 eV and 2.5 eV for implantation energies 150 keV and 100 keV, respectively. These results are comparable to that measured for Ar implanted into germanium target.

Keywords: thermal desorption spectroscopy, gallium arsenide, ion implantation

INTRODUCTION

Gallium arsenide (GaAs), compound of gallium and arsenic, forming a zinc blend structure gray crystals, was synthesized in 1920s [1]. Its density is approximately 5.32 g/cm^3 and melting point is 1511 K [2]. GaAs was recognized as a good candidate for electronics material due its large electron mobility (9000 cm^2/Vs), larger than those of crystalline silicon. Moreover, GaAs is characterised by a wide direct band-gap of ~1.42 eV (some sources give slightly higher value of ~1.52 eV [3]). Due to its light-emitting and electromagnetic properties combined with high carrier mobility, GaAs could be considered as one of the basic semiconductor material for the production photoconductors, light emitters, laser diodes and other high-power high-speed microwave devices [4,5]. GaAs based devices are characterised by better performance at high temperatures compared to standard microelectronics materials. Moreover, it offers lower power consumption combined with radiation damage resistance. Other advantages to be mentioned are: controllable bandwidth and desirable optical absorption [2]. GaAs is a material that could be successfully used as a base of photovoltaic cells - it is reported that the material could increase substantially the efficiency of such cells up to 44.7% [6], as there is a strict correlation between the solar cell efficiency and the value of the band gap [7]. It is well known that using of ion implantation technology results in creation of additional energy levels, also in GaAs[8]. Moreover, changing irradiation conditions allows precise control of introduced levels [9]. It is also known that electron jump mechanism plays an important role in charge transfer in H^+ irradiated GaAs. Changes of the conductivity with temperature are strictly related to the annealing of different radiation induced defects [10].

Thermal desorption spectroscopy (TDS) also known as thermal programmed desorption (TPD) is a well established technique enabling studies of substance release either from the surface or from the subsurface layers of solids as a function of the sample temperature. Such measurement may give gain to the knowledge about

the sample lattice imperfections like vacancies and their clusters as well as to help to determine diffusion coefficients. TDS is frequently combined with ion implantation in order to study the disorder introduced to solid target by ion bombardment. A typical field of interest is the retention of impurities both in classical (fission) nuclear reactor materials as well as in those used in still developed fusion devices like Be, W, Zr or graphite [11-14].

The TDS usually makes use of light gases like hydrogen, deuterium and helium. It should be mentioned here that ion implantation with gaseous elements may lead to formation of cavities and bubbles filled with introduced gas. This happens both in metals and in semiconductors. The formation of bubbles found its applications for impurities gettering [15] and in ''ion cut'' or ''smart-cut'' thin layer transfer process invented (for silicon) by Bruel [16,17]. This technique has also been extended to GaAs [18,19].

Numerous reports [20-25] concerning production of helium bubbles in silicon by high fluence ion irradiation were delivered by several groups. These approaches made use of altering the bombardment energy from keV up to MeV range as well as other important parameters like fluencies, implantation and annealing temperatures. Moreover, co-implantation with other gases was also applied. It should be mentioned here that the release of heavier inert gases (including Ar [26-29], Xe [30-32] and Kr [33]) implanted with different energies was also studied, however desorption activation energies were usually higher for such gases than for lighter ones.

As it was already mentioned, a majority of gas bubble formation studies (including those employing TDS approach) was performed for Si or Si-based materials, being the cornerstone of electronics. Germanium, characterised by large electron mobility also, attracted attention of scientists. It was found that 60 keV He irradiation leads to the formation of 1 nm bubbles [34]. A high fluence (10^{17} cm^{-2}) H^+ implantation followed by annealing (T > 700 K) resulted in surface blistering and even crater formation for large enough doping [35]. Sudden release of Ar implanted with energies 100 and 150 keV were observed for temperatures in the range 790-850 K while the corresponding desorption activiation energies were equal 3.2 eV and 2.2 eV, respectively [36]. On the other hand, the release of He from Ge has a form of wide bands [37].

There is a plenty of reports about formation of gas bubbles and blisters due to ion implantation of GaAs sometimes followed by annealing, an excellent review could be found in [38]. GaAs surface blistering as a result of ion implantation was reported for H [39,40] deuterium [41] or H and He co-implantation [42]. Thermal desorption spectroscopy combined with Auger spectroscopy and low energy electron diffraction was successfully used for studies of H_2S desorption on gallium arsenide surface [43]. A similar approach was also applied to research an adsorption/desorption of chlorine on GaAs [44], proving a preferential replacement reaction between Cl and As. A combination of X-ray photoelectron spectroscopy (XPS), and time-of-flight secondary ion mass spectrometry (TOF-SIMS) was used to study adsorption and decomposition pathways of heavier organic compounds like 1-propanethiol on a GaAs(100) surface [45]. On the other hand, there is very little information concerning thermal release of gases implanted into GaAs target, especially compared to the mentioned earlier case of Si or Ge. This paper is aimed at filling this gap.

The paper presents investigations of thermal desorption of argon implanted into GaAs target with energies 100 keV and 150 keV in order to determine the desorption activation energy for relatively heavy projectile. The other aim is to check possible changes of GaAs surface morphology after annealing and gas release. Implantation fluencies were similar to that in the previous cases of silicon bombardment (i.e. 1×10^{16} cm^{-2}). Thermal desorption spectra were collected for linear heating profiles with ramp rates in the range 0.3 K/s up to 1.2 K/s. Analysis (according to Redhead approach) of the release peak shift with the ramp rate was performed in order to calculate the desorption activation energy. The results are discussed and compared to that obtained for other targets. A brief description of the experimental setup is also presented for the sake of completeness.

EXPERIMENTAL

GaAs wafers of orientation 100 were implanted with Ar^+ ions with energies 150 keV and 100 keV. Irradiation fluencies were chosen as 10^{16} cm^{-2}, as in the previously considered case of Ar to Si implantation [29]. All implantation were done at room temperature. Implantation current density was set

below 1 mA/cm^2 to prevent excessive sample heating and sputtering.

The equipment, namely the TDS spectrometer used for gas release measurements was described in details previously [29-33]. A short description is given here for completeness. It should be also mentioned here that the setup is still developed for best possible performance. The schematic view of the experimental setup is shown in Figure 1. Main body of the spectrometer is the stainless steel vacuum chamber (diameter of ~35 cm) equipped with several flanges, ports and feedthroughs. The chamber contains small sample holder attached to the Boralectric HTR1002 (Momentive, Strongsville OH, USA) ceramic-covered heater. The holder-heater unit is shielded by steel and molybdenum screens in order to prevent excessive heating of the chamber walls as well as to decrease condensation of vapors produced by the sample on internal surfaces of the chamber. The heater is powered by a programmable power supply EA-PS 8080T (EA-Electro-Automatik GmbH, Viersen, Germany). Such configuration enables fast and reliable sample heating with different profiles and rates up to ~1600 K. It should be mentioned here that this limit is mainly due to using the K-type thermocouple. The accuracy of temperature measurement is of order 10 K, and was estimated using pyrometer enabling measurements in central or peripheric parts of the heater. Both the thermocouple and the programmable power supply are connected via Hewlett-Packard 34970A data acquisition switch to the personal computer running the custom made proportional–integral–derivative (PID) algorithm based software controlling the experimental setup. During all presented measurements a linear profile of sample heating was deployed:

$$T(t) = T_o + \beta t \quad (1)$$

where: T_o denotes the initial (usually room) temperature and β is the heating ramp rate (in the considered case in the range 0.3 K/s up to 1.2 K/s).

The signal corresponding to implanted isotopes (or to the substrate atoms) is measured by the quadruple mass spectrometer QMG 220 M (Pfeiffer Vacuum, Asslar, Germany) with secondary electron multiplier detector. The quadruple mass spectrometer is controlled by Quadera^{TM} software package, enabling saving and analyzing of spectra.

The vacuum system in its presents form consists of the two independent pairs of turbomolecular and rotary vane forevacuum pumps – one of them provides vacuum in the main vessel, the other in the mass spectrometer tube. The above mentioned two compartments of the TDS spectrometer could be separated from each other using the gate valve system when necessary, e.g. during

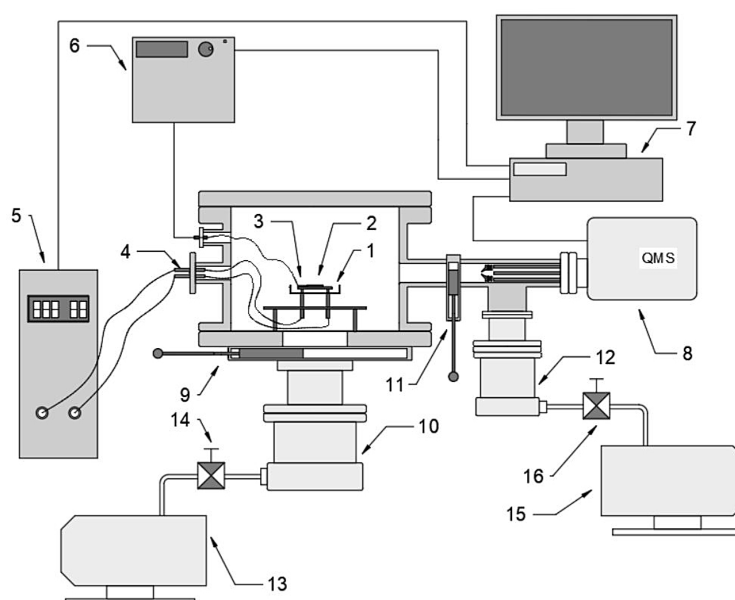

Fig. 1. Schematic drawing of the experimental setup: 1 – sample heater, 2 – sample, 3 – K-type thermocouple, 4 – electrical feedthrough, 5 – programmable power supply, 6 – data acquisition switch, 7 – PC-class microcomputer, 8 – quadruple mass spectrometer, 9, 11 – gatevalves , 10,12 – turbomolecular pumps, 13,15 – rotary vane forevacuum pumps, 14,16 – forevacuum gate valves

the heater annealing or static measurements. The double pump set allow achieving the pressure base pressure of 10^{-8} mbar. Closing the gate valve 9 during the measurement makes vapors desorbed from the sample pass through the gate valve 11 towards the quadruple mass spectrometer, which enables the use of very small samples of surface 0.25 cm^2 or even smaller.

RESULTS

Figure 2 presents depth profiles of Ar implanted into GaAs as well as of vacancies produced in the target material. The simulations were done using SRIM software package [46]. The projected implantation ranges were 75 nm (100 keV) and 110 nm (150 keV) with the stragglings 35 nm and 50 nm, correspondingly. These results are very similar to that obtained in the case of Ar implanted into Ge [36]. However, the maximum dopant concentration are smaller due to the fact that the fluence is 10^{16} cm^{-2} in the case of GaAs target. Having in mind the difference of fluences, the maximal dopant concentrations are almost the same in both cases. The defected GaAs layer thickness is ~80% smaller than the projected range of Ar^+ ions. As in the case of Ar bombarded Ge one deals with rather thick defected layer buried under a very thin (~20 nm) top unmodified GaAs layer. One has to have in mind that the concentration of defects in GaAs is lower than that obtained germanium for the same irradiation conditions.

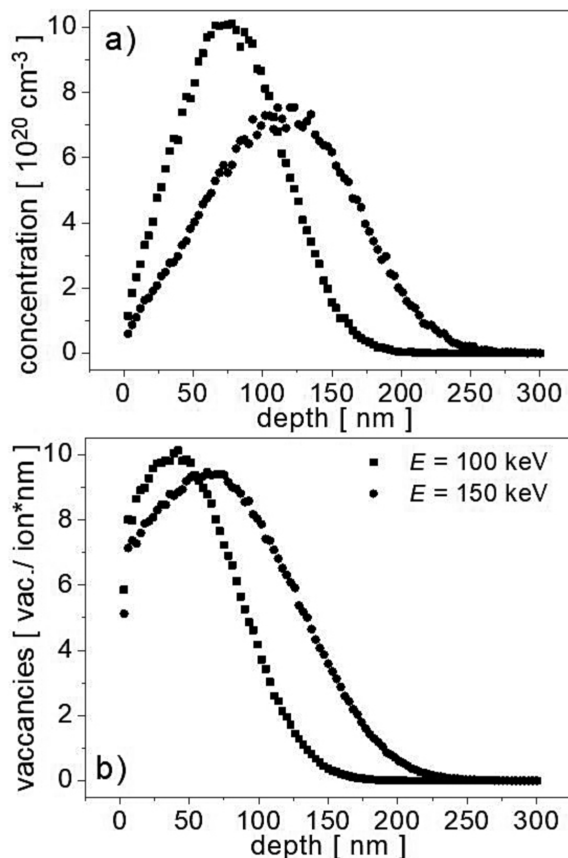

Fig. 2. Implanted Ar concentration (a) and vacancies distributions (b) in GaAs calculated using the SRIM package

The similarity of these two cases could be also seen in the TDS spectra. Those for GaAs are presented in Figure 3 for implantation energies 100 keV and 150 keV. One can see that the main release of Ar form the sample has the form of very narrow peaks (FWHM ~20 K, estimated after subtracting the background signal). One should have in mind that these abrupt emission take place for much higher temperatures (1100 – 1180 K) than in the case of Ge target (below 850 K) characterized by much lower melting point. It should be mentioned here that in the case of Ar implanted Si a different scenario of Ar was observed [29]. Very sharp TDS peak was registered for temperatures in the range 930-940 K. It corresponded to Ar release from gas filled cavities. The second release had a form of a very broad band and its position depended on the implantation energy – for 50 keV [28] that peak was registered earlier (i.e. for lower temperatures) than that corresponding to rapid emission from cavities/bubbles. The slow emission was assigned to the Ar release due to the diffusion of gas dispersed in the Si lattice. As it was already said the Ar emission from GaAs has the form of sharp peaks (its positions are gathered together in the Table 1). However, a strong more or less constant signal corresponding to Ar for temperatures starting form ~450 K cannot be simply neglected without any further tests. As in the case of Ge samples background emission test (i.e. without implanted sample) were performed, for several chosen heating rates in order to check, whether a sudden Ar release is observed that could interfere with the signal from the sample and make the activation energy estimations much harder. An example of the background signal is presented in Figure 4. The intensity of the background signal corresponds to that seen in the flat or slowly ascending part of TDS signal measured for implanted sample. Fortunately, no sudden releases of Ar was observed. The background emission comes from the atmospheric Ar trapped in various parts of the experimental setup, including

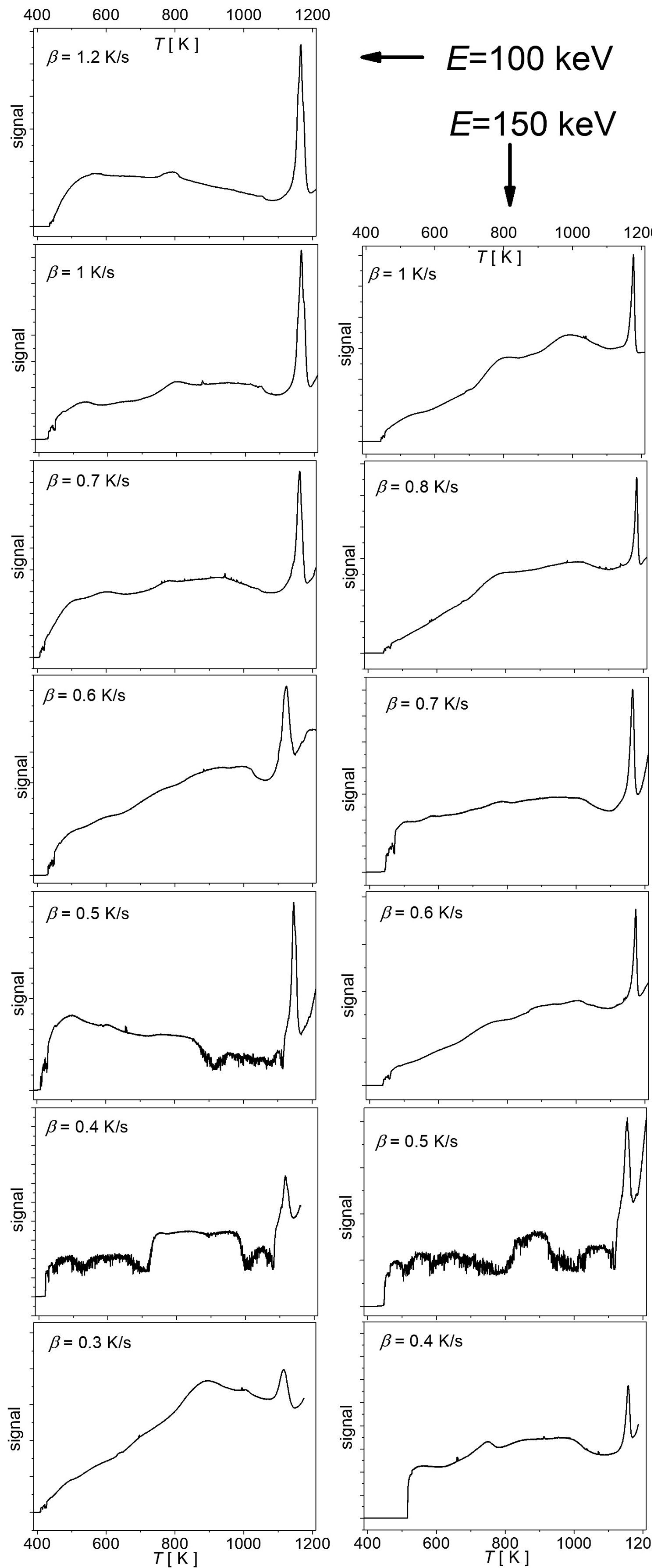

Fig. 3. TDS spectra collected for the 100 keV Ar^+ (left column) and 150 keV Ar^+ implanted samples (right column)

Table 1. Temperatures of Ar release (temperatures corresponding to the TDS spectra peaks) and desorption activation energies for the two implantation energies

E [keV]	β [K/s]	T_p [K]	Q [eV]
100	0.3	1115	2.6 ± 0.7
	0.4	1117	
	0.5	1146	
	0.6	1124	
	0.7	1160	
	1	1165	
	1.2	1166	
150	0.4	1154	3.6 ± 1.2
	0.5	1153	
	0.6	1173	
	0.7	1165	
	0.8	1181	
	1	1178	

the heater itself, heater shielding and the chamber walls. All these setup parts release Ar from their surfaces as their temperature increases during the TDS spectrum measurement. It is rather extremely hard to get rid of that strong atmospheric Ar signal, as the chamber is opened every time the sample is changed. Using a transfer gate, manipulators combined with the whole device heat treatment could be considered as a hypothetical solutin of that problem.

The main release of Ar from GaAs is most probably related to the formation of stable gas-filled bubbles. They are results of coalescence of vacancies or their small clusters, sometimes containing trapped Ar atoms, as it was in the case of He in germanium lattice [21,47]. As temperature increases bubbles become more and more pressurized as the pressure riches a critical point and gas is released at it was observed both for heavier inert gases in Si [29] and Ge [36].

As one can see in Figures 3 (and in Table 1) the peak temperatures increase as the heating ramp rate rises. The shift is stronger than in the case of Ar release form Ge, especially in the case of E = 100 keV. It is approximately 50 K and it corresponds to much smaller b increase (from 0.3 K/s up to 1.2 K/s). This shift is comparable to that observed for He desorption from implanted Ge [39]. Unfortunately, one can see that the increase is not as smooth as in the above mentioned cases – a kind of staggering of unclear origin is observed. Some role may be played by the fact that signs of fast thermal decomposition of GaAs could be seen for temperatures above 1150 K. It should be mentioned that the mentioned process of thermal decomposition is reported in wide range of temperatures starting from ~900 K [48]. Figure 5 presents mass signals corresponding to main isotopes of Ga (69 a.m.u.) and As (75 a.m.u.) which are related to partial pressure of each species. For lower temperatures one can see the preferential evaporation of Ga. However, for temperatures higher than 1150 K the situation changes and evaporation of As prevails, which is in good agreement with data presented in [48].

As in previous cases one can see that the TDS peaks for deeper implanted samples are registered for higher temperatures. The average shift is rather small, it is approximately 15 K, much smaller than for heavy inert gases (Xe, Kr) implanted into Si.

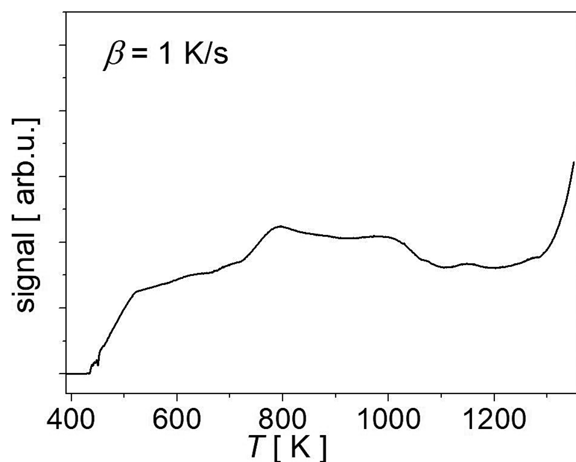

Fig. 4. The example of Ar^+ background TDS signal (without any sample in the spectrometer)

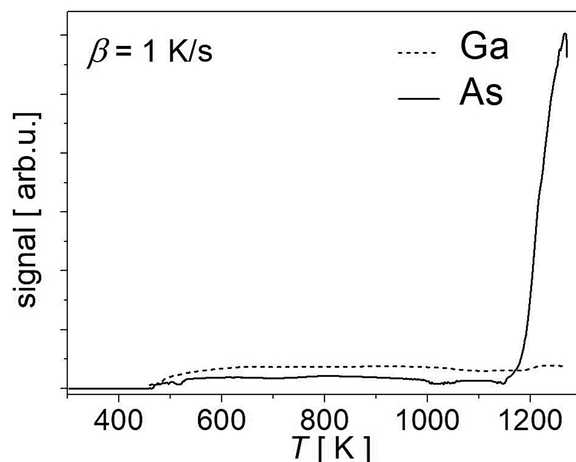

Fig. 5. TDS signals corresponding to main isotopes of Ga (69 a.m.u.) and As (75 a.m.u.)

Estimation of the desorption activation energies could be performed using analysis of the peak shifts according to Redhead's approach [49]. The desorption process could be described by Polanyi-Wigner equation:

$$\frac{dn}{dt} = -\gamma(n,T)n^m \exp\left(-\frac{Q(n,T)}{kT}\right) \quad (2)$$

where: n is the surface density of the desorbing atoms, m is the kinetic order of desorption, k is the Boltzmann constant, Q is the desorption activation energy and g is a pre-exponential factor.

Redhead method could be used under assumption that the desorption process is of the first order (m = 1) and the pre-exponential factor g and the desorption energy Q do not depend on the coverage. In such case the Polanyi-Wigner equation is:

$$\frac{dn}{dt} = -\gamma n \exp\left(-\frac{Q}{kT}\right) \quad (3)$$

Having in mind that the linear heating profile is assumed (see formula (1)), and denoting by T_p the temperature corresponding to the maximal signal (the peak of the TDS spectrum), one gets to the relation:

$$\frac{1}{T_p} = \frac{k}{Q}\ln\left(\frac{T_p^{\,2}}{\beta}\right) + \frac{k}{Q}\ln\left(\gamma\frac{k}{Q}\right) \quad (4)$$

which is a consequence of equation $d^2n/dt^2 = 0$ for the peak temperature. For the more advanced analyses one can use a 'complete analyses method' or a 'leading edge method' [50]. These methods assume that g and Q depend on the surface coverage/surface density.

As can seen in (3), the diffusion activation energy Q could be obtained by calculating the slope of the $1/T_p$ vs. ln ($T_p^{\,2}/b$) plot. Such plots are shown in Figure 6. One can see that the slopes of the straight lines fitted to experimental points obtained for the two implantation energies are similar. The estimations of the desorption activation energy are presented also in Table 1. It should be mentioned that the pre-exponential factor g can be also obtained from Eq. (4). The desorption activation energy for E = 100 keV is 2.6 ± 0.7 eV and 3.6 ± 1.2 eV for that for E = 150 keV. Similar values were obtained previously for Ar implanted into Ge. Unfortunately, the uncertainty is rather large in considered case and reaches even 30%. Nevertheless, one may expect that desorption activation energy for light inert gas like He will be much smaller than that measured for Ar (in Ge target it has a value of 0.75 eV). In the case of Si target it was observed that Q increases both with atomic mass of the gas-projectile and its atomic radius. On the other hand, in the case of Ge implanted with Kr the desorption activation energy was smaller than that for Ar – this effect could be explained by larger amount of disorder that is introduced at a shallower layer in the case of heavier projectile.

CONCLUSIONS

In the paper the investigation of thermal desorption of Ar implanted into GaAs samples with energies 100 keV and 150 keV is presented. The TDS spectra were collected applying linear ramp rate heating profiles with b changing form 0.3 up to 1.2 K/s. In all cases single narrow Ar release peak was observed in temperature ranges 1100 K up to 1180 K (much higher than in the case of Ar implanted into Ge). A strong background Ar

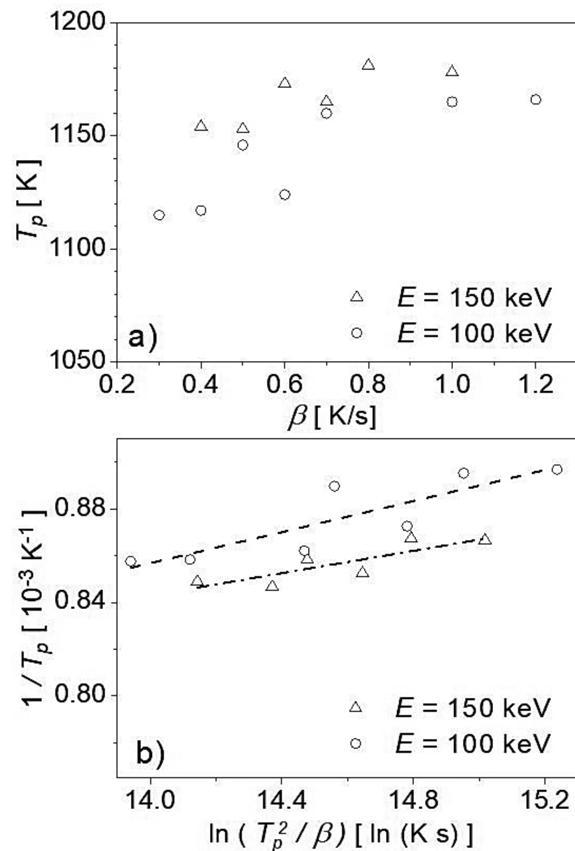

Fig. 6. Dependence of release temperature T_p on heating rate b (a) and Redhead's plots ($1/T_p$ vs. ln ($T_p^{\,2}/b$)) for samples implanted with 100 keV Ar^+ and 150 keV Ar^+ GaAs samples (b)

signal was registered due to the atmospheric Ar release from different parts of the TDS spectrometer. Nevertheless, the single abrupt emission form the sample is most probably the effect of the release of Ar trapped into pressurized bubbles, created as a result of vacancy clusters coalescence. The peak shift analysis allowed estimation of desorption activation energy. These values are approximately 3.6 ± 1.2 eV for E = 150 keV and 2.6 ± 0.7 eV for E = 100 keV, comparable to those measured for Ar implanted into Ge.

Acknowledgements

The publication of the paper is supported by the “Excellence in Science” program of the Polish Ministry of Education and Science (*“Międzynarodowa Konferencja “Implantacja jonowa i inne zastosowania jonów i elektronów ION’2022”*).

REFERENCES

1. Goldschmidt V.M., Crystal structure and chemical constitution Trans Faraday Soc 1929; 25: 253-283.
2. Akinlami J.O., Ashamu A.O., Optical properties of GaAs , J. Semicond., 2013; 34(3): 032002.
3. Sze S. M.,. Ng K. K, Physics of semiconductor devices. 3rd ed., John Wiley and Sons., 2007.
4. Baca A.G.,. Ashby C.I.H, Fabrication of GaAs Devices, The Institution of Engineering and Technology, 2005.
5. Liou J. J., Schwierz F. , RF MOSFET: recent advances, current status and future trends Solid-State Electron. 2003; 47(11): 1881-1895.
6. Wegierek P., Pietraszek J., Analysis of the Influence of Annealing Temperature on Mechanisms of Charge Carrier Transfer in GaAs in the Aspect of Possible Applications in Photovoltaics Acta Physica Polonica A 2019; 136(2): 299-302.
7. Luque A., Hegedus S., Handbook of Photovoltaic Science and Engineering, 2nd Ed., John Wiley & Sons, 2011.
8. Wegierek P., Pietraszek J., Application of polyenergy implantation with H + ions for additional energy levels formation in GaAs dedicated to photovoltaic cells, Archives Of Electrical Engineering 2019; 68(4): 925-931.
9. Kowalski M., Partyka J., Wegierek P., Żukowski P., Komarov F.F., Jurchenko A.V., Freik D. , Frequency-dependent annealing characteristics of the implant-isolated GaAs layers, Vacuum 2005; 78(2-4): 311-317.
10. Węgierek P., Billewicz P. , Research on Jump Mechanism of Electric Charge Transfer Probability in Gallium Arsenide Irradiated with H + Ion, Przegląd Elektrotechniczny 2012; 88(11b): 364-365.
11. Makepeace C., Pardanaud C., Roubin P., Borodkin I. Ayres C., Coad P., Baron-Wiechec A., Jepu I., Heinola K., Widdowson A., Lozano-Perez S. and J.E.T. Contributors, The effect of beryllium oxide on retention in JET ITER-like wall tiles, Nuclear Materials and Energy 2019; 19: 346-351.
12. Zhang M., Deng K., Wei F., Wu X., Du L., Liu W., Adsorption and Desorption of Tritium on/from Nuclear Graphite, ACS Omega 2022; 7(1): 752-760.
13. Oya M., Shimada M., Taylor C. N., Kobayashi M. I., Nobuta Y., Yamauchi Y., Oya Y., Ueda Y., Hatano Y., Deuterium retention in tungsten irradiated by high-dose neutrons at high temperature, Nuclear Materials and Energy 2021; 27: 100980.
14. Ma M., Liang L., Tang B., Xiang W., Wang Y., Cheng Y., Tan X., Decomposition kinetics study of zirconium hydride by interrupted thermal desorption spectroscopy, Journal of Alloys and Compounds 2015; 645: S217-S270.
15. Hirose R., Kadono T., Onaka-Masada A., Okuyama R., Kobayashi K., Suzuki A., Y. Koga, Kurita K., Proximity gettering design of silicon wafers using silicon hydride and hydrocarbon mixture molecular ion implantation technique, Materials Science in Semiconductor Processing 2021; 135: 106063.
16. Bruel M., Silicon on insulator material technology, Electron. Lett. 1995; 31(14): 1201-1202.
17. Bruel M., Application of hydrogen ion beams to Silicon On Insulator material technology, Nucl. Instrum. Methods Phys. Res. B 1996; 108(3): 313-319.
18. Zheng Y., Moran P. D., Guan Z. F., Lau S. S., Hansen D. M., Kuech T. F., Haynes T. E., Hoechbauer T. and Nastasi M., Transfer of n-type GaSb onto GaAs substrate by hydrogen implantation and wafer bonding, J. Electron. Mater. 2000; 29: 916-920.
19. Izuhara T., Levy M., and Osgood, Jr. R. M., Direct wafer bonding and transfer of 10-μm-thick magnetic garnet films onto semiconductor surfaces, Appl. Phys. Lett. 2000; 76: 1261- 1263.
20. Oliviero E., David M. L., Beaufort M. F., Barbot J. F., van Veen A., On the effects of implantation temperature in helium implanted silicon, Appl. Phys. Lett. 2002; 81(22): 4201-4203.
21. Corni F., Calzolari G., Gambetta F., Nobili C., Tonini R., Zapparoli M., Evolution of vacancy-like defects in helium-implanted (100) silicon studied by thermal desorption spectrometry, Materials Science and Engineering B 2000; 71(1-3): 207-212.
22. Cerofolini G.F., Calzolari G., Corni F., Frabboni S., Nobili C., Ottaviani G., Tonini R., Thermal desorption spectra from cavities in helium-implanted silicon, Phys. Rev. B 2000; 61(15): 10183.

23. Godey S., Ntsoenzok E., Sauvage T., van Veen A., Labohm F., Beaufort M.F., Barbot J.F., Helium desorption from cavities induced by high energy 3He and 4He implantation in silicon Materials Science and Engineering B 2000; 73(1-3): 54-59.
24. Desgardin P., Barthe M.-F., Ntsoenzok E., Liu C.-L., Modifications of He implantation induced cavities in silicon by MeV silicon implantation, Applied Surface Science 2006; 252(9): 3231-3236.
25. Lau W. M., Bello I. , Huang L. J., Feng X., Vos M., Mitchell I .V ., Argon incorporation in Si(100) by ion bombardment at 15–100 eV, J. Appl. Phys. 1993; 74(12): 7101.
26. Filius A., van Veen A., Bijkerk K. R., and Evans J. H., The retention of Ar in low energy high fluence Ar-Irradiated Mo and Sim Radiat. Eff. 1989; 108(1): 1-8.
27. Hanada R., Saito S., Nagata S., Yamaguchi S., Shinozuka T., Fujioka I., TDS and RBS studies of Ar lmplanted to Si, Mat. Sci. Forum 1995; 196-201: 1375.
28. Drozdziel A., Wojtowicz A., Turek M., Pyszniak K., Maczka D., Slowinski B., Yushkevich Y.V. and Zuk J., Thermal Desorption Studies of Ar + Implanted Silicon, Acta Phys. Pol. A 2014; 125(6): 1400-1403.
29. Werner M.,. van den Berg J. A, Armour D. G., Carter G., Feudel T., Herden M., Bersani M., Giubertoni D., Ottaviano L., Bongiorno C., Mannino G., Bailey P., and. Noakes, T. C. Q Shallow BF2 implants in Xe-bombardment-preamorphized Si: theinteraction between Xe and F, Appl. Phys. Lett. 2005; 86(15): 151904.
30. Barbieri P. F., Landers R., and Marques F.C., Electronic and structural properties of implanted xenon in amorphous silicon, Appl. Phys. Lett. 2007; 90(16): 164104.
31. Turek M., Droździel A., Pyszniak K., Wójtowicz A., Vaganov Y., Termodesorpcja ksenonu implantowanego do krzemu, Przeglad Elektrotechniczny 2018; 94(7): 157-161.
32. Turek M., Droździe1 A., Wójtowicz A., Filiks J., Pyszniak K., Mączka D., Yuschkevich Y., Thermal Desorption of Krypton Implanted into Silicon, Acta Phys. Pol. A 2017; 132(2): 249-253.
33. David M-L., Alix K., Pailloux F., Mauchamp V., Couillard M., Botton G. A., and Pizzagalli L., In situ controlled modification of the helium density in single helium-filled nanobubbles, Journal of Applied Physics 2014; 115(12): 123508.
34. Yang F., Zhang X.-X. ,Ye T.-C. and Zhuang S.-L., The Investigation on Surface Blistering of Ge Implanted by Hydrogen under the Low Temperature Annealing, Journal of The Electrochemical Society 2011; 158(12): H1233.
35. Turek M., Droździel A., Pyszniak K., Vaganov Y.A., Termodesorpcja argonu implantowanego do germanu, Przegląd Elektrotechniczny 2020; 96(8): 126-130.
36. Turek M., Droździel A., Pyszniak K., Prucnal S., Żuk J., Vaganov Yu., Thermal Desorption of He Implanted into Ge, Acta Physica Polonica A 136(2), 2019, 285-289
37. Collino R. R., Blister Formation And Layer Transfer Of N-Implanted GaAs, PhD Thesis, The University of Michigan, 2010.
38. Gawlik G., Jagielski J., and Piatkowski B., GaAs on. Si: towards a low-temperature smart-cut. Technology, Vacuum 2003; 70(2-3): 103-105.
39. Webb M., Jeynes C., Gwilliam R. M., Tabatabaian Z., Royle A., and Sealy B. J., The influence of the ion implantation temperature and the flux on smart-cut© in GaAs. Nucl. Instrum. Methods Phys. Res. B 2005; 237(1-2): 193-196.
40. Webb M., Jeynes C., Gwilliam R., Too P., Kozanecki A., Domagala J.,
41. Royle A., and Sealy B., The influence of the ion implantation temperature and the dose rate on smart-cut (c) in GaAs, Nucl. Instrum. Meth. B 2005; 240(1-2): 142-145.
42. Radu I., Szafraniak I., Scholz R., Alexe M., and Gösele U., GaAs on Si heterostructures obtained by He and/or H implantation and direct wafer bonding, J. Appl. Phys. 2003; 94(13): 7820-7825.
43. Chung C., Yi S. I., Weinberg W. H., Adsorption state of hydrogen sulfide on the GaAs (001)-(4×2) surface, J. Vac. Sci. Technol. A 1997; 15(3): 1163-1167.
44. Mokler S. M., Watson P. R., Ungier L. and Arthur J. R. Adsorption and thermal desorption of chlorine from GaAs(100) surfaces, Journal of Vacuum Science & Technology B 1992; 10(6): 2371-2377.
45. Donev S., Brack N., Paris N. J., Pigram P. J., Singh N. K., Usher B. F., Surface Reactions of 1-Propanethiol on GaAs(100), Langmuir 2005; 21(5): 1866-1874.
46. Ziegler J. F., Ziegler M. D., Biersack J. P., SRIM - The Stopping and Range of Ions in Mater Nucl. Instr. Meth. B 2010; 268(11-12): 1818-1823.
47. Corni F., Nobili C., Ottaviani G., Tonini R., Calzolari G., Cerofolini G. F. and Queirolo G., Helium in silicon: Thermal-desorption investigation of bubble precursors, Phys. Rev. B 1997; 56: 7331.
48. Haynes T.E.,. Chu W.K, Aselage T.L., Picraux S.T., Initial decomposition of GaAs during rapid thermal annealing, Appl. Phys. Lett. 1986; 49(11): 666-668.
49. Redhead P.A, Thermal desorption of gases, Vacuum 1962; 12(4): 203-211.
50. de Jong A.M. and Niemantsverdriet J.W., Thermal desorption analysis: Comparative test of ten commonly applied procedures, Surface Sciences 1990; 233 (3): 355-365.